

Electronic structure of the neutral silicon-vacancy center in diamond

B. L. Green,^{1,2,*} M. W. Doherty,³ E. Nako,^{1,2} N. B. Manson,³ U. F. S. D’Haenens-Johansson,⁴ S. D. Williams,⁵ D. J. Twitchen,⁵ and M. E. Newton^{1,2}

¹*Department of Physics, University of Warwick, Coventry, CV4 7AL, UK*

²*EPSRC Centre for Doctoral Training in Diamond Science and Technology, UK*

³*Laser Physics Centre, Research School of Physics and Engineering,*

Australian National University, Australian Capital Territory 2601, Australia

⁴*Gemological Institute of America, 50 W 47th St, New York, NY 10036, USA*

⁵*Element Six Limited, Global Innovation Centre, Fermi Avenue, OX11 0QR, UK*

The neutrally-charged silicon vacancy in diamond is a promising system for quantum technologies that combines high-efficiency, broadband optical spin polarization with long spin lifetimes ($T_2 \approx 1$ ms at 4 K) and up to 90 % of optical emission into its 946 nm zero-phonon line. However, the electronic structure of SiV^0 is poorly understood, making further exploitation difficult. Performing photoluminescence spectroscopy of SiV^0 under uniaxial stress, we find the previous excited electronic structure of a single ${}^3\text{A}_{1u}$ state is incorrect, and identify instead a coupled ${}^3\text{E}_u - {}^3\text{A}_{2u}$ system, the lower state of which has forbidden optical emission at zero stress and so efficiently decreases the total emission of the defect: we propose a solution employing finite strain to form the basis of a spin-photon interface. Isotopic enrichment definitively assigns the 976 nm transition associated with the defect to a local mode of the silicon atom.

Optically-accessible solid state defects are promising candidates for scalable quantum information processing [1, 2]. Diamond is the host crystal for two of the most-studied point defects: the negatively-charged nitrogen vacancy (NV^-) center [3], and the negatively-charged silicon vacancy (SiV^-) center [4]. NV^- has been successful in a broad range of fundamental [5, 6] and applied [7–9] quantum experiments, with spin-photon [10] and spin-spin [11] entanglement protocols well-established. The superior photonic performance of SiV^- , with >70 % of photonic emission into its zero phonon line (ZPL), has enabled it to make a rapid impact in photonic quantum platforms [12, 13]. However, SiV^- possesses poor spin coherence lifetimes due to phononic interactions in the ground state (GS) [14], requiring temperatures of <100 mK to achieve $T_2 \approx 400$ μs without decoupling [15].

Recent work on SiV^0 , the neutrally-charged silicon vacancy in diamond, has demonstrated that it combines high-efficiency optical spin polarization [16] with long spin lifetimes ($T_2 \approx 1$ ms at 4 K [17]) and a high degree of coherent emission: the defect potentially possesses the ideal combination of SiV^- and NV^- properties. Exploitation of these promising properties is hindered by poor understanding of the defect’s electronic structure. Electron paramagnetic measurements (EPR) of SiV^0 indicate it has a spin triplet ${}^3\text{A}_{2g}$ GS and D_{3d} symmetry [18], with the silicon atom residing on-axis in a split-vacancy configuration [Fig 1, inset]. Optically-excited EPR measurements directly relate the SiV^0 spin system to a zero phonon line (ZPL) at 946 nm [16]: optical absorption experiments and density functional theory (DFT) calculations have assigned the ZPL excited state (ES) to ${}^3\text{A}_{1u}$ symmetry [19, 20]. Temperature-dependent PL measurements indicate the presence of an optically-inactive state below the luminescent excited state [19].

The advances in exploitation of NV^- and SiV^- have been driven by a concerted effort in the fundamental understanding of the physics of the centers themselves. In this Letter, we employ photoluminescence (PL) spectroscopy to study an ensemble of SiV^0 under applied uniaxial stress, and show that the previous assignment of a single excited state ${}^3\text{A}_{1u}$ is incorrect. We find that the 946 nm excited state is ${}^3\text{E}_u$, with a ${}^3\text{A}_{2u}$ state approximately 6.8 meV below it. The latter transition is forbidden by symmetry at zero stress and therefore efficiently reduces the emission intensity of unstrained SiV^0 centers at low temperature. However, under finite strain, the proposed electronic structure enables the possibility of resonantly exciting spin-selective optical transitions between the ${}^3\text{A}_{2g}$ GS and ${}^3\text{A}_{2u}$ ES. The latter state is shown definitively to participate in the optical spin polarization mechanism of SiV^0 . Finally, we demonstrate that the 976 nm transition associated with SiV^0 [16], previously hypothesised to be a strain-induced transition [20], is actually a pseudo-local vibrational model (LVM) of SiV^0 primarily involving the silicon atom.

We apply uniaxial stress to a diamond crystal grown by chemical vapour deposition: the crystal was doped with silicon during growth to create SiV^- and SiV^0 . Uniaxial stress was applied to the sample using a home-built ram driven by pressurized nitrogen gas. PL measurements were collected under excitation at 785 nm as a function of applied stress in both the $\langle 111 \rangle$ and $\langle 1\bar{1}0 \rangle$ directions (see [21] for detail). We measured spectra for all four combinations of excitation and detection polarization parallel (π) and perpendicular (σ) to the stress axis. We found that the spectra are essentially invariant to excitation polarization [21]. This is likely due to the excitation mechanism being polarization-insensitive photoionization, as our 785 nm (1.58 eV) excitation laser

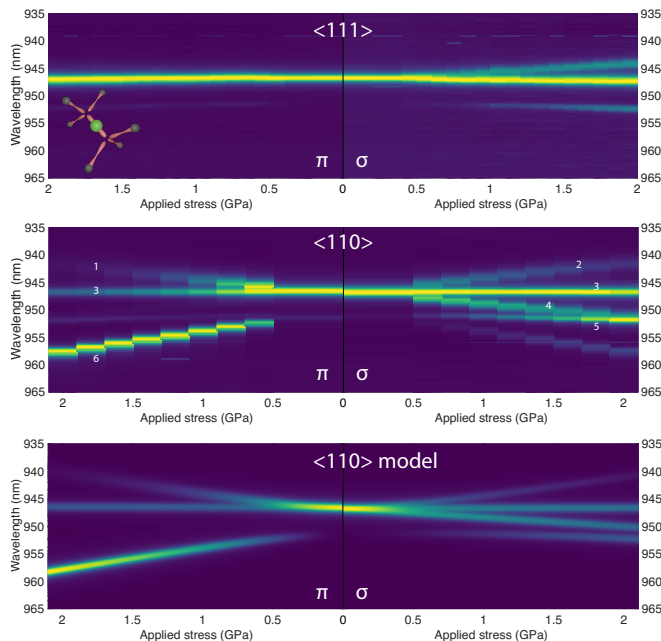


FIG. 1. SiV^0 photoluminescence spectra at 80 K as a function of applied stress along $\langle 111 \rangle$ (top) and $\langle 110 \rangle$ (middle). In each case, π (σ) indicates detection polarization parallel (perpendicular) to the stress direction. The transition at 946 nm splits into components 1–4 under $\langle 110 \rangle$ stress, with thermalisation between the components observed at high stress indicating electronic degeneracy. A pair of stress-induced transitions (5,6) originate at approximately 951 nm. Inset, top: the geometric form of SiV^0 , with the Si atom on-axis in the split-vacancy configuration. Bottom: simulation of the $\langle 110 \rangle$ stress spectra using the model described in main text.

is above the 830 nm (1.50 eV) photoionization threshold of SiV^0 [22]. We can thus focus on analysing just the spectra for the two detection polarizations (π , σ) arising from a single excitation polarization (π).

The problem of uniaxial stress applied to a trigonal defect in a cubic crystal has been described several times [23–25], so we summarise the results for transitions to an orbital singlet GS, as found in SiV^0 . In both $\langle 111 \rangle$ and $\langle 110 \rangle$ applied stress, the orientational degeneracy of the defect is lifted into two classes of orientation, classified by the angle between their high-symmetry axis and the uniaxial stress axis. For an orbital singlet-to-singlet ($A \leftrightarrow A$) transition, only one transition per orientation is possible: when taking into account both orientation classes, we expect a maximum of two transitions per spectrum. In the orbital singlet-to-doublet ($A \leftrightarrow E$) case, two transitions per orientation are possible, leading to a maximum of four transitions per spectrum. $\langle 111 \rangle$ stress does not remove the electronic degeneracy of the E_x, E_y orbitals for the orientation parallel to the applied stress, and hence a maximum of three transitions are expected.

For uniaxial stress applied along the $\langle 111 \rangle$ axis, the 946 nm ZPL splits into three transitions, two of which are

almost degenerate but which possess different emission polarization [Fig. 1]. This is consistent with the $A \leftrightarrow E$ case described earlier. Under $\langle 110 \rangle$ uniaxial stress, we identify four distinct components originating at the ZPL, again consistent with an $A \leftrightarrow E$ transition. The intensities of the different components varies as a function of applied stress, confirming the presence of electronic degeneracy in the excited state. For both stress directions, we observe additional lower-energy transitions originating at ≈ 951 nm: the transitions gain intensity as a function of stress [Fig. 1]. We measure only two components, indicating the presence of an additional orbital singlet state. At a constant applied stress of $\sigma_{\langle 110 \rangle} = 1.3$ GPa, decreasing the temperature increases the intensity of the stress-induced transitions at the expense of the ZPL transitions. Therefore, we conclude the additional A state lies below the excited E state, rather than above the ground ${}^3A_{2g}$.

In order to construct a model of the excited state behavior, we must establish the origin of the lower-energy A state. There are three possible origins: (1) spin-orbit (SO) fine structure arising from the E level; (2) Jahn-Teller (JT) vibronic structure arising from the E level; and (3) a totally independent A level. An SO interaction of 6.5 meV (≈ 1.57 THz) is inconsistent with the magnitude of the SO interaction in SiV^- (250 GHz [4]) and GeV^- (1.06 THz [26]) and would yield additional A and E states (as in NV^- ES [27]) and hence we reject this possibility. A JT distortion would place the A state above the E and hence is inconsistent with experiment. Additionally, the piezospectroscopic parameters describing the singlet and doublet states are significantly different [21], as would be expected if they arise from distinct electronic states [28]. We conclude that the singlet is an additional electronic state and is not derived from the doublet. Experimentally, we find the singlet transitions are polarized in pure σ for $\langle 111 \rangle$ stress, and pure σ , π for $\langle 110 \rangle$ stress [Fig. 1]: this identifies the A level as possessing Γ_1 symmetry in the lowered C_s symmetry of the defect under stress [21].

Building on previous numerical descriptions of a coupled $E - A$ system in trigonal symmetry [28], we construct a full analytical treatment of this problem. For a given SiV sub-ensemble under applied stress, the coupled Hamiltonian is

$$H = \begin{pmatrix} W + \alpha' & \gamma^c & \beta^c \\ \gamma^c & \alpha + \beta & \gamma \\ \beta^c & \gamma & \alpha - \beta \end{pmatrix} \quad (1)$$

where α , β , γ (α') describe the response to stress of the E (A) state, β^c and γ^c describe coupling between the two states, and W is the energy difference between the states at zero stress. $\alpha^{(l)}$, $\beta^{(c)}$ and $\gamma^{(c)}$ are functions of the state-dependent piezospectroscopic parameters and are linear in applied stress. The eigenenergies of this Hamiltonian can be parameterised as follows (see [21] for

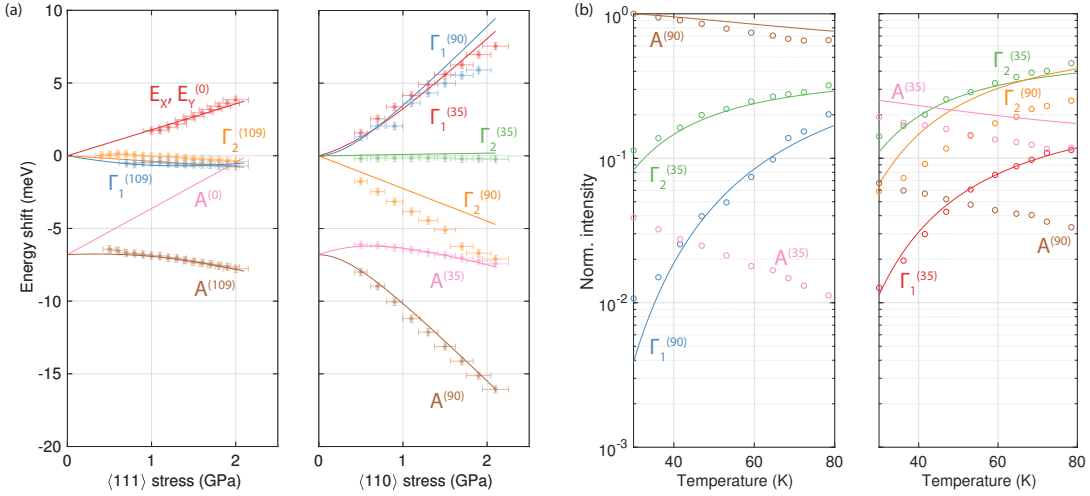


FIG. 2. Comparison of experimental data (dots) with the coupled $E - A$ model (solid lines). Transitions are labelled with the state (A and Γ_1, Γ_2 for the E state) and the angle between the symmetry axis of the sub-ensemble and the stress axis (in degrees). (a) Transition energies as a function of applied stress in the $\langle 111 \rangle$ (left) and $\langle 110 \rangle$ (right) directions. Theoretical intensity of the $A^{(0)}$ transition is 0, and the line was not observed in experiment. (b) Transition intensities at an applied $\langle 110 \rangle$ stress of 1.3 GPa as a function of sample temperature. Data are given in both π (left) and σ (right) detection polarizations. The data have been normalized to the most intense transition.

derivation)

$$\begin{aligned}
 E(A) &= \frac{1}{2} (\alpha + \Delta + W + \alpha') \\
 &\quad - \frac{1}{2} \left[(\alpha + \Delta - W - \alpha')^2 + 4\Omega^2 \right]^{1/2} \\
 E(\Gamma_1) &= \frac{1}{2} (\alpha + \Delta + W + \alpha') \\
 &\quad + \frac{1}{2} \left[(\alpha + \Delta - W - \alpha')^2 + 4\Omega^2 \right]^{1/2} \quad (2) \\
 E(\Gamma_2) &= \alpha - \Delta
 \end{aligned}$$

where Δ is the stress splitting of the E level in the absence of the coupling to the A level and Ω is the coupling between the A level and the E state that also has Γ_1 symmetry under C_s stress. The intensities of the corresponding lines in detection polarization p are

$$\begin{aligned}
 I_p(A) &= Z^{-1} e^{-E(A)/k_B T} I_{1p} \sin^2 \frac{\phi}{2} \\
 I_p(\Gamma_1) &= Z^{-1} e^{-E(\Gamma_1)/k_B T} I_{1p} \cos^2 \frac{\phi}{2} \quad (3) \\
 I_p(\Gamma_2) &= Z^{-1} e^{-E(\Gamma_2)/k_B T} I_{2p}
 \end{aligned}$$

where I_{1p} and I_{2p} are intensities of p -polarization components of the Γ_1 and Γ_2 transitions (given in [21]), $\phi = \arctan \frac{2\Omega}{\alpha + \Delta - W - \alpha'}$ is the angle describing the coupling between the A and the Γ_1 substate of the E state, and Z is the partition function.

The result of a least-squares fit of this model simultaneously to the experimental $\langle 110 \rangle$ and $\langle 111 \rangle$ spectra as a function of stress is given in Fig. 2(a): piezospectroscopic parameters are detailed in the SI [21]). The

output of the model was tested by comparing it to the transition intensities of spectra measured as a function of temperature at a fixed $\sigma_{\langle 110 \rangle} = 1.3$ GPa [Fig. 2(b)]. The ordering and behavior of all transitions matches the experiment and hence we accept the coupled $E - A$ model as a suitable description of the SiV^0 excited state.

There are several reasons why the model fit is not perfect. Intrinsic inhomogeneous stress will introduce nonlinearities into the line-shifts at low stress; small misalignments or non-uniaxial stress will modify the shift-rates from those taken into account by the model, which will be exacerbated if these effects are different in the two stress directions. Finally, Jahn-Teller interactions in the E state, and pseudo-Jahn Teller interactions between the E and A are not taken into account within the model: high quality absorption data under stress are required to confirm the presence of these interactions, and the low concentration of SiV^0 in the present sample prohibits absorption measurements.

With the excited states' orbital degeneracy and symmetry under stress confirmed, we now reconcile our observations with the electronic model of SiV^0 . The EPR-active ${}^3A_{2g}$ GS arises from the molecular orbital (MO) configuration $a_{1g}^2 a_{2u}^2 e_u^4 e_g^2$ ($\equiv e_g^2$ in the hole picture, used henceforth), along with ${}^1E_g, {}^1A_{1g}$ [20]. The previously-assigned ${}^3A_{1u}$ ES arises from $e_u^1 e_g^1$ [19], in addition to ${}^1A_{1u}, {}^1A_{2u}, {}^1E_u, {}^3A_{2u}$ and 3E_u states. As e_g^2 and $e_u^1 e_g^1$ are the two lowest-energy one-electron configurations [20], we identify the doubly-degenerate ES observed under stress with the 3E_u ($e_u^1 e_g^1$) state.

The requirement of applied stress for observation of the singlet transitions [Fig. 1] indicates that the transi-

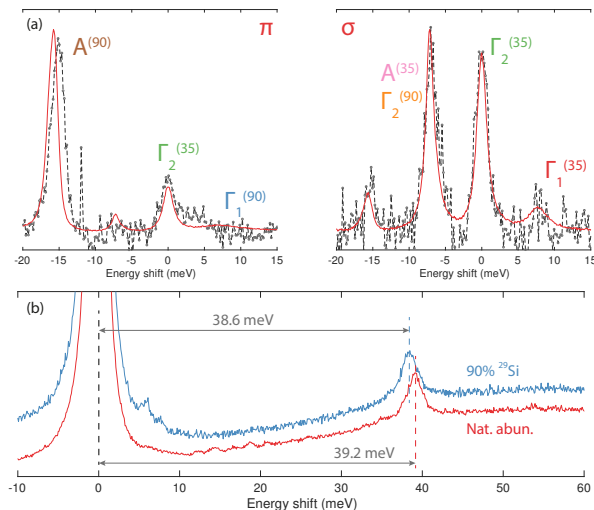


FIG. 3. (a) Comparison of PL measurements of the 946 nm and associated stress-induced transitions (solid lines) with the 976 nm local mode (dots). Measurements collected at $\sigma_{(110)} = 2.1$ GPa for both π (left) and σ detection polarization. Individual transitions are labeled as in Fig. 2. (b) Effect of isotopic enrichment on the 976 nm local vibrational mode. The mode shifts from $\Omega_0 = 39.2$ meV in natural abundance material (92% ^{28}Si) to $\Omega^* = 38.6$ meV in a sample enriched with 90% ^{29}Si . Treating the mode as a simple harmonic oscillation of the silicon atom yields $\Omega^* = 38.6$ meV, matching experiment. ZPLs have been fixed at zero for clarity.

tions are forbidden by orbital symmetry but not spin. As the only $S = 1$ state arising from the e_g^2 configuration, we assume that the GS of this transition is the EPR-active $^3A_{2g}$: the singlet is then restricted by symmetry selection rules to $^3A_{1g}$, $^3A_{2g}$ and $^3A_{2u}$. The observed Γ_1 symmetry under stress may be derived from both A_{1g} and A_{2u} in D_{3d} ; however, only the latter is consistent with the electronic model and hence we assign the symmetry $^3A_{2u}$ ($e_u^1 e_g^1$). We identify this state with the ≈ 5 meV state observed in temperature-dependent PL measurements, where the intensity of the ZPL was shown to decrease with decreasing temperature [19].

In addition to the purely electronic transitions discussed above, the PL spectrum of SiV^0 also exhibits a small feature at 976 nm [16]. In our measurements, we find that the energy shift of the transition under stress is essentially identical 946 and 951 nm transitions [Fig. 3(a)] [21]. As the line is at lower energy than the associated ZPLs we associate it with a pseudo-LVM in the common GS. This observation is incompatible with previous density functional theory (DFT) calculations suggesting that this transition is a stress-induced electronic transition between a 3E_g ES and the $^3A_{2g}$ GS [20].

To investigate the participation of Si in the pseudo-LVM, PL measurements of a sample grown with isotopically enriched silicon dopant were performed: we find that the vibration frequency drops from 39.2 meV

in a natural abundance sample ($>90\%$ ^{28}Si) to 38.6 meV in a sample enriched with 90% ^{29}Si [Fig. 3(b)]. Modelling the vibration as a simple harmonic oscillator, the mode frequency under isotopic enrichment is given by $\Omega^* = \Omega_0 \sqrt{m^*/m_0}$, where m^* is the effective mass of the isotopic enrichment, and Ω_0 , m_0 are the mode frequency and effective mass in a natural abundance sample, respectively. Applying this model yields $\Omega_{\text{model}}^* = 38.6$ meV, matching the experimental value. This confirms that the LVM is primarily due to oscillation of the Si within the vacancy ‘cage’, and is only weakly coupled to the bulk. Finally, the symmetry of the LVM may be addressed. The similar polarization behavior of the 946 and 976 nm transitions [Fig 3(a)] indicates an a_{1g} mode. However, only e_u or a_{2u} silicon oscillations participate in pseudo-LVM modes [29]: in both these cases, the overall mode symmetry $^3A_{2g} \otimes \Gamma_{\text{LVM}}$ becomes *ungerade* and thus vibronic transitions from both 3E_u and $^3A_{2u}$ excited states are forbidden by parity. We may reconcile the spectroscopic data with the model only by considering symmetry-lowering distortions. For example, under instantaneous symmetry-lowering distortions from $D_{3d} \rightarrow C_{3v}$ due to (pseudo-)Jahn-Teller distortions in the ES, the a_{2u} mode becomes a_1 and the vibronic transition is no longer forbidden. We observe no sharp mode related to the e_u oscillation of the silicon. A similarly complex situation is encountered in SiV^- , where two pseudo-LVMs have been identified at 40 and 64 meV [4]. Studies of the latter indicate that its frequency is well-approximated by a simple harmonic oscillator model [30] and essentially involves only the silicon atom, as we find for the 39 meV mode of SiV^0 . However, experimental measurements assign the 64 meV mode to a_{2u} symmetry [30, 31] through polarized single-center studies, whereas recent hybrid-DFT calculations assign the mode e_u symmetry and argue that the 40 meV mode is not an LVM [29]. Further work is required to definitively identify the vibrational states of SiV in both charge states.

With knowledge of the excited state symmetries and behavior under stress, we may re-analyse recent measurements of the spin polarization behavior [16, 17]. The latter measurement identifies significant spin polarization at approximately 951 nm (Fig. S9 [17]): in light of our new results on the stress-induced optical transition at 951 nm, we understand that the measurement was performed on a strained ensemble, and interpret its visibility in an absorption spectrum as a direct transition from the $^3A_{2g}$ ground state to the $^3A_{2u}$ state [Fig. 4(a)]. As the measurements were completed by reading out spin polarization from the $^3A_{2g}$ GS, this is direct evidence that the $^3A_{2u}$ ES is involved in the spin polarization mechanism. At 4 K, $k_B T \approx 0.3$ meV and hence thermal excitation from $^3A_{2u}$ to 3E_u is negligible. The spin polarization mechanism must therefore either involve interactions with both the 3E_u and $^3A_{2u}$ states, or via phonon relaxation from the 3E_u state through $^3A_{2u}$ [Fig 4(a)].

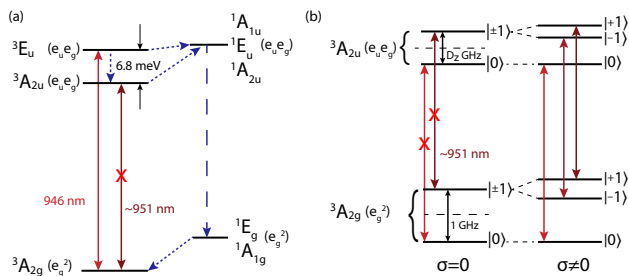


FIG. 4. (a) The electronic structure of SiV^0 proposed as a result of uniaxial stress measurements. The ordering and relative energies of the spin singlets is not known. Electronic configurations are described in the hole picture i.e. $e_u e_g \equiv a_{2u}^2 a_{1g}^2 e_u^3 e_g^3$. (b) Proposed scheme for spin-dependent initialization and readout of the 951 nm transition under a small applied strain. D_z is not known.

Information on the relative ordering of the singlet states is required for a full description of the spin polarization mechanism [21].

The thermal interaction of the 3E_u and ${}^3A_{2u}$ states poses a problem for the use of SiV^0 as a photonic resource, as the intensity of the 946 nm transition decreases with decreasing temperature due to thermal depopulation from 3E_u into ${}^3A_{2u}$: typically, <20 K is required to isolate spin-conserving optical transitions in diamond [32, 33]. For small ($\lesssim 0.3$ GPa) stresses applied perpendicular to the symmetry axis, the intensity and frequency of the 951 nm transition is quadratic in stress: the stress will also remove the $m_s = \pm 1$ spin degeneracy in the spin triplets. Under stress, the spin-conserving optical transitions between ${}^3A_{2g}$ GS and ${}^3A_{2u}$ ES are no longer forbidden [Fig. 4(b)], and in conjunction with the spin polarization mechanism in SiV^0 may enable spin-dependent optical initialization and readout at low magnetic field. To resolve spin-dependent optical transitions, we require the difference in the zero-field splitting of the GS and ES to be larger than the inhomogeneous linewidth of the transitions themselves. Implementation of this scheme would form the foundation of an SiV^0 spin-photon interface [10]. Future work should include monitoring strained SiV^0 centers in both EPR and resonant PL to determine the effect of strain on the spin-spin interactions in both the orbital singlet states, and measurement of single centers under strain to identify spin-conserving optical transitions.

We thank B. G. Breeze at the University of Warwick Spectroscopy Research Technology Platform for helpful discussion and assistance with experiments. BLG gratefully acknowledges the financial support of the Royal Academy of Engineering. This work is supported by EPSRC Grants No. EP/L015315/1 and EP/M013243/1, and ARC Grants No. DE170100169 and DP140103862.

* b.green@warwick.ac.uk; Corresponding Author

- [1] I. Aharonovich, D. Englund, and M. Toth, *Nat. Photonics* **10**, 631 (2016).
- [2] L. J. Rogers, K. D. Jahnke, T. Teraji, L. Marseglia, C. Müller, B. Naydenov, H. Schauffert, C. Kranz, J. Isoya, L. P. McGuinness, and F. Jelezko, *Nat. Commun.* **5**, 4739 (2014).
- [3] M. W. Doherty, N. B. Manson, P. Delaney, F. Jelezko, J. Wrachtrup, and L. C. L. Hollenberg, *Phys. Rep.* **528**, 1 (2013).
- [4] L. J. Rogers, K. D. Jahnke, M. W. Doherty, A. Dietrich, L. P. McGuinness, C. Müller, T. Teraji, H. Sumiya, J. Isoya, N. B. Manson, and F. Jelezko, *Phys. Rev. B* **89** (2014).
- [5] T. Gaebel, M. Domhan, I. Popa, C. Wittmann, P. Neumann, F. Jelezko, J. R. Rabeau, N. Stavrias, A. D. Green-tree, S. Praver, J. Meijer, J. Twamley, P. R. Hemmer, and J. Wrachtrup, *Nat. Phys.* **2**, 408 (2006).
- [6] B. Hensen, H. Bernien, A. E. Dréau, A. Reiserer, N. Kalb, M. S. Blok, J. Ruitenber, R. F. L. Vermeulen, R. N. Schouten, C. Abellán, W. Amaya, V. Pruneri, M. W. Mitchell, M. Markham, D. J. Twitchen, D. Elkouss, S. Wehner, T. H. Taminiau, and R. Hanson, *Nature* **526**, 682 (2015).
- [7] P. Maletinsky, S. Hong, M. S. Grinolds, B. Hausmann, M. D. Lukin, R. L. Walsworth, M. Loncar, and A. Yacoby, *Nat. Nanotechnol.* **7**, 320 (2012).
- [8] Y. Wang, F. Dolde, J. Biamonte, R. Babbush, V. Bergholm, S. Yang, I. Jakobi, P. Neumann, A. Aspuru-Guzik, J. D. Whitfield, and J. Wrachtrup, *ACS Nano* **9**, 7769 (2015).
- [9] L. Rondin, J.-P. Tetienne, T. Hingant, J.-F. Roch, P. Maletinsky, and V. Jacques, *Reports Prog. Phys.* **77**, 056503 (2014).
- [10] E. Togan, Y. Chu, A. S. Trifonov, L. Jiang, J. Maze, L. Childress, M. V. G. Dutt, a. S. Sørensen, P. R. Hemmer, A. S. Zibrov, and M. D. Lukin, *Nature* **466**, 730 (2010).
- [11] H. Bernien, B. Hensen, W. Pfaff, G. Koolstra, M. S. Blok, L. Robledo, T. H. Taminiau, M. Markham, D. J. Twitchen, L. Childress, and R. Hanson, *Nature* **497**, 86 (2013).
- [12] A. Sipahigil, R. E. Evans, D. D. Sukachev, M. J. Burek, J. Borregaard, M. K. Bhaskar, C. T. Nguyen, J. L. Pacheco, H. A. Atikian, C. Meuwly, R. M. Camacho, F. Jelezko, E. Bielejec, H. Park, M. Lončar, and M. D. Lukin, *Science* **354**, 847 (2016).
- [13] A. Sipahigil, K. D. Jahnke, L. J. Rogers, T. Teraji, J. Isoya, A. S. Zibrov, F. Jelezko, and M. D. Lukin, *Phys. Rev. Lett.* **113**, 113602 (2014).
- [14] S. Meesala, Y.-I. Sohn, B. Pingault, L. Shao, H. A. Atikian, J. Holzgrafe, M. Gundogan, C. Stavrakas, A. Sipahigil, C. Chia, M. J. Burek, M. Zhang, J. L. Pacheco, J. Abraham, E. Bielejec, M. D. Lukin, M. Atature, and M. Loncar, arXiv:1801.09833.
- [15] D. D. Sukachev, A. Sipahigil, C. T. Nguyen, M. K. Bhaskar, R. E. Evans, F. Jelezko, and M. D. Lukin, *Phys. Rev. Lett.* **119**, 223602 (2017).
- [16] B. L. Green, S. Mottishaw, B. G. Breeze, A. M. Edmonds, U. F. S. D’Haenens-Johansson, M. W. Doherty, S. D. Williams, D. J. Twitchen, and M. E. Newton, *Phys. Rev. Lett.* **119**, 096402 (2017).

- [17] B. C. Rose, D. Huang, Z.-H. Zhang, A. M. Tyryshkin, S. Sangtawesin, S. Srinivasan, L. Loudin, M. L. Markham, A. M. Edmonds, D. J. Twitchen, S. A. Lyon, and N. P. de Leon, arXiv:1706.01555.
- [18] A. M. Edmonds, M. E. Newton, P. M. Martineau, D. J. Twitchen, and S. D. Williams, *Phys. Rev. B* **77**, 245205 (2008).
- [19] U. F. S. D’Haenens-Johansson, A. Edmonds, B. L. Green, M. E. Newton, G. Davies, P. Martineau, R. Khan, and D. Twitchen, *Phys. Rev. B* **84**, 245208 (2011).
- [20] A. Gali and J. R. Maze, *Phys. Rev. B* **88**, 235205 (2013).
- [21] See Supplemental Material at <http://abc> for description of the experimental geometry and apparatus, comparison of spectra with different input polarizations, derivation of the analytical solutions to the coupled stress Hamiltonian, the model parameters used to generate the simulation, and detail on the computation of transition intensities.
- [22] L. Allers and A. T. Collins, *J. Appl. Phys.* **77**, 3879 (1995).
- [23] A. E. Hughes and W. A. Runciman, *Proc. Phys. Soc.* **90**, 827 (1967).
- [24] G. Davies and M. E. R. Hamer, *Proc. R. Soc. London Ser. A* **348**, 285 (1976).
- [25] L. J. Rogers, M. W. Doherty, M. S. J. Barson, S. Onoda, T. Ohshima, and N. B. Manson, *New J. Phys.* **17**, 013048 (2015).
- [26] Y. N. Palyanov, I. N. Kupriyanov, Y. M. Borzdov, and N. V. Surovtsev, *Sci. Rep.* **5**, 14789 (2015).
- [27] P. Delaney, J. C. Greer, and J. A. Larsson, *Nano Lett.* **10**, 610 (2010).
- [28] G. Davies, *J. Phys. C Solid State Phys.* **12**, 2551 (1979).
- [29] E. Londero, G. Thiering, A. Gali, and A. Alkauskas, arXiv:1605.02955v2.
- [30] A. Dietrich, K. D. Jahnke, J. M. Binder, T. Teraji, J. Isoya, L. J. Rogers, and F. Jelezko, *New J. Phys.* **16**, 113019 (2014).
- [31] L. J. Rogers, K. D. Jahnke, M. H. Metsch, A. Sipahigil, J. M. Binder, T. Teraji, H. Sumiya, J. Isoya, M. D. Lukin, P. Hemmer, and F. Jelezko, *Phys. Rev. Lett.* **113**, 263602 (2014).
- [32] K. M. C. Fu, C. Santori, P. E. Barclay, L. J. Rogers, N. B. Manson, and R. G. Beausoleil, *Phys. Rev. Lett.* **103**, 256404 (2009).
- [33] L. Nicolas, T. Delord, P. Huillery, E. Neu, and G. Hétet, arXiv:1804.05583.

Supplemental Material

EXPERIMENTAL DETAIL

We have measured SiV^0 in a sample grown by chemical vapour deposition. The sample has faces $\langle 1\bar{1}0 \rangle$, $\langle 111 \rangle$ and $\langle 11\bar{2} \rangle$. Photoluminescence experiments were performed in backscatter geometry i.e. $Z(\psi_e\psi_d)\bar{Z}$ in Porto notation, where ψ_e and ψ_d are the excitation and detection E vector, respectively [Fig. S1]. As discussed in the main text, we find no dependence of the spectra on the input polarization ψ_e [Fig. S2], and so all spectra are presented for both detection polarizations only.

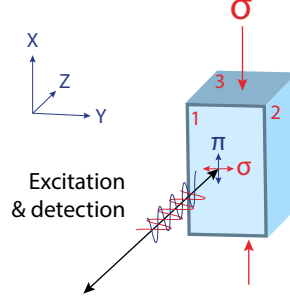


FIG. S1. Geometry for stress experiments: the excitation / detection are backscattered for all measurements. Faces 1, 2, 3 are $[1\bar{1}\bar{1}]$, $[\bar{1}1\bar{2}]$, $[110]$ ($[\bar{1}1\bar{2}]$, $[110]$, $[1\bar{1}\bar{1}]$) for $\langle 110 \rangle$ ($\langle 111 \rangle$) stress, respectively. The electric field vector for excitation and detection is either parallel (π) or perpendicular (σ) to the stress axis.

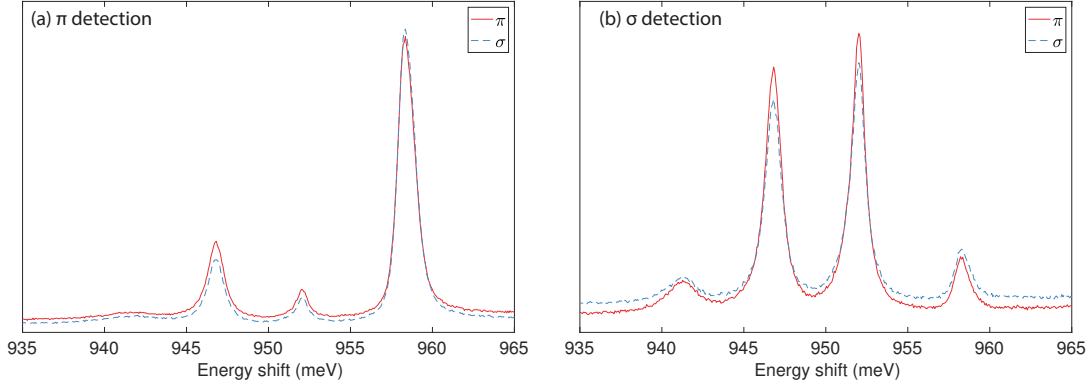


FIG. S2. Comparison of raw spectra collected at an applied $\langle 110 \rangle$ stress of 2.1 GPa. Spectra are given for (a) π detection polarization and (b) σ detection polarization: the two input polarizations are given in each case. No significant difference between input polarizations is visible at this or any other stress value measured.

Uniaxial stress was applied to the sample using a home-built ram driven by high pressure nitrogen gas and controlled by a Bronkhorst flow controller. The stress cell was mounted into an Oxford Instruments Optistat for low temperature measurements. All measurements were performed using a 785 nm laser (1.58 eV). The parameters used to generate the model in the main text are given in Table S1.

TABLE S1. Model parameter values used to generate the simulation given in the main text. All parameters are in meV GPa^{-1} except W , which is given in meV.

\mathcal{A}_1	\mathcal{A}_2	\mathcal{B}	\mathcal{C}	\mathcal{A}'_1	\mathcal{A}'_2	\mathcal{B}	\mathcal{C}	W
-0.077	0.93	-1.0	-0.24	0.97	1.1	-4.7	-1.1	-6.8

DERIVATION OF THE STRESS HAMILTONIAN SOLUTIONS

Let the stress Hamiltonian of A and E states in the absence of coupling be

$$H_{\text{uncoupled}} = \begin{pmatrix} W + \alpha' & 0 & 0 \\ 0 & \alpha + \beta & \gamma \\ 0 & \gamma & \alpha - \beta \end{pmatrix}. \quad (\text{S1})$$

The Hamiltonian describing the coupling interaction between the states is

$$H_{\text{coupled}} = \begin{pmatrix} 0 & \gamma^c & \beta^c \\ \gamma^c & 0 & 0 \\ \beta^c & 0 & 0 \end{pmatrix} \quad (\text{S2})$$

The eigenbasis of the coupling-free $H_{\text{uncoupled}}$ is

$$\begin{pmatrix} 1 & 0 & 0 \\ 0 & \cos[\frac{\theta}{2}] & -\sin[\frac{\theta}{2}] \\ 0 & \sin[\frac{\theta}{2}] & \cos[\frac{\theta}{2}] \end{pmatrix} \quad (\text{S3})$$

Transforming into this basis, the matrix representation of the total Hamiltonian $H = H_{\text{uncoupled}} + H_{\text{coupled}}$ is

$$H = \begin{pmatrix} W + \alpha' & \gamma^c \cos[\frac{\theta}{2}] + \beta^c \sin[\frac{\theta}{2}] & \beta^c \cos[\frac{\theta}{2}] - \gamma^c \sin[\frac{\theta}{2}] \\ \gamma^c \cos[\frac{\theta}{2}] + \beta^c \sin[\frac{\theta}{2}] & \alpha + \beta \cos[\theta] + \gamma \sin[\theta] & \gamma \cos[\theta] - \beta \sin[\theta] \\ \beta^c \cos[\frac{\theta}{2}] - \gamma^c \sin[\frac{\theta}{2}] & \gamma \cos[\theta] - \beta \sin[\theta] & \alpha - \beta \cos[\theta] - \gamma \sin[\theta] \end{pmatrix} \quad (\text{S4})$$

The expressions for α , β and γ are defined by the symmetry of the center (D_{3d}), and are given below following [S1, S2]:

$$\begin{aligned} \alpha &= \mathcal{A}_1(\sigma_{XX} + \sigma_{YY} + \sigma_{ZZ}) + 2\mathcal{A}_2(\sigma_{YZ} + \sigma_{ZX} + \sigma_{XY}) \\ \beta &= \mathcal{B}(2\sigma_{ZZ} - \sigma_{XX} - \sigma_{YY}) + \mathcal{C}(2\sigma_{XY} - \sigma_{YZ} - \sigma_{ZX}) \\ \gamma &= \sqrt{3}\mathcal{B}(\sigma_{XX} - \sigma_{YY}) + \sqrt{3}\mathcal{C}(\sigma_{YZ} - \sigma_{ZX}) \end{aligned} \quad (\text{S5})$$

Here, the σ_{ij} refer to elements of the stress matrix expressed in the crystal axes. α' is defined as α but with \mathcal{A}'_1 , \mathcal{A}'_2 to reflect the different piezospectroscopic response of the doublet and singlet states. Similarly, β^c and γ^c are as β , γ with \mathcal{B}^c and \mathcal{C}^c . W is the difference in energy between the doublet and singlet excited states. The reduced matrix elements $\mathcal{A}_1^{(l)}$, $\mathcal{A}_2^{(l)}$, $\mathcal{B}^{(c)}$, and $\mathcal{C}^{(c)}$ have the same form as given by [S3].

We now construct the Hamiltonian for each sub-ensemble for each stress direction.

(111) stress

The angle between the defect symmetry axis z and the applied stress axis $\hat{\sigma}$ is denoted θ_σ . For (111) stress applied to a trigonal defect, we need only consider two cases: the ‘unique’ orientation with $\theta_\sigma = 0^\circ$; and the three equivalent orientations with $\theta_\sigma = 109^\circ$.

The stress matrix is constructed as $\sigma_{ij} = \sigma(\hat{\sigma}.i) \times (\hat{\sigma}.j)$, where i, j run over the crystal axes X, Y, Z , and is subsequently rotated into each orientation frame. For the representative orientations 1 & 2 [see Table S2] with the substitution $\theta = \lim_{x \rightarrow \beta} \frac{\gamma}{\beta}$, the Hamiltonian parameters are:

	α	$\beta \equiv \Delta$	γ	α'	$\beta^c \equiv \Omega$	γ^c
0° sub-ensemble	$\sigma(\mathcal{A}_1 + 2\mathcal{A}_2)$	0	0	$\sigma(\mathcal{A}'_1 + 2\mathcal{A}'_2)$	0	0
109° sub-ensemble	$\sigma(\mathcal{A}_1 - \frac{2}{3}\mathcal{A}_2)$	$\frac{4}{3}\mathcal{C}\sigma$	0	$\sigma(\mathcal{A}'_1 - \frac{2}{3}\mathcal{A}'_2)$	$\frac{4}{3}\mathcal{C}^c\sigma$	0

Finally, the eigenvalues of the resulting Hamiltonian are as above with $\Delta \equiv \beta$ and $\Omega \equiv \beta^c$:

	α	Δ	α'	Ω
0° sub-ensemble	$\sigma(\mathcal{A}_1 + 2\mathcal{A}_2)$	0	$\sigma(\mathcal{A}'_1 + 2\mathcal{A}'_2)$	0
109° sub-ensemble	$\sigma(\mathcal{A}_1 - \frac{2}{3}\mathcal{A}_2)$	$\frac{4}{3}\mathcal{C}\sigma$	$\sigma(\mathcal{A}'_1 - \frac{2}{3}\mathcal{A}'_2)$	$\frac{4}{3}\mathcal{C}^c\sigma$

TABLE S2. The four possible orientations of a trigonal center in a T_d lattice.

	x	y	z
1	$[\bar{1}\bar{1}0]$	$[\bar{1}1\bar{2}]$	$[111]$
2	$[\bar{1}10]$	$[\bar{1}\bar{1}2]$	$[\bar{1}\bar{1}\bar{1}]$
3	$[110]$	$[1\bar{1}2]$	$[1\bar{1}\bar{1}]$
4	$[\bar{1}\bar{1}0]$	$[\bar{1}12]$	$[11\bar{1}]$

 $\langle 110 \rangle$ stress

For $\langle 110 \rangle$ applied stress, we need again only consider two cases: the pair of orientations with $\theta_\sigma = 35^\circ$; and the pair of orientations with $\theta_\sigma = 90^\circ$. For the representative orientations 1 & 3 [see Table S2], the Hamiltonian parameters are:

	α	$\beta \equiv \Delta$	γ	α'	$\beta^c \equiv \Omega$	γ^c
35° sub-ensemble	$\sigma(\mathcal{A}_1 + \mathcal{A}_2)$	$\sigma(-\mathcal{B} + \mathcal{C})$	0	$\sigma(\mathcal{A}'_1 + \mathcal{A}'_2)$	$\sigma(-\mathcal{B}^c + \mathcal{C}^c)$	0
90° sub-ensemble	$\sigma(\mathcal{A}_1 - \mathcal{A}_2)$	$\sigma(-\mathcal{B} - \mathcal{C})$	0	$\sigma(\mathcal{A}'_1 - \mathcal{A}'_2)$	$\sigma(-\mathcal{B}^c - \mathcal{C}^c)$	0

As found in the $\langle 111 \rangle$ case, $\Delta \equiv \beta$ and $\Omega \equiv \beta^c$.

INTENSITIES OF STRESS-SPLIT TRANSITIONS

As discussed above and in the main text, for photoluminescence stress measurements performed with an ionizing input beam, the spectra are essentially invariant to input polarization and therefore the expected intensities therefore reduce to the case encountered in absorption measurements.

The expressions for the intensities given in the main text require the intensities of each transition at zero stress in the experimental geometry. The analytical values have been calculated in several places [S3, S4]. However, the sample used in our experiment has $\{111\}$, $\{11\bar{2}\}$ and $\{1\bar{1}0\}$ faces: the standard tables give intensities for $\langle 110 \rangle$ or $\langle 001 \rangle$ readout under $\langle 1\bar{1}0 \rangle$ stress. In Table S3 we give the zero-stress intensities for both $\langle 111 \rangle$ and $\langle 110 \rangle$ stress, including intensities of transitions when measured with detection polarization $\psi_d \parallel \langle 11\bar{2} \rangle$ under $\sigma \parallel \langle 110 \rangle$, as found in our experiment.

TABLE S3. Analytical intensities for different detection polarizations for an $E \leftrightarrow A_2$ transition at a trigonal center, following [S5]. For $\langle 110 \rangle$ stress, the σ polarization values are calculated for a perpendicular direction of $\langle 11\bar{2} \rangle$, as employed in our experiment.

Stress	Orientation	Sym.	Energy	π	σ
	① 0°	E_X, E_Y	$\mathcal{A}_1 + 2\mathcal{A}_2$	0	1
$\langle 111 \rangle$	②	$E_X (\Gamma_1)$	$\mathcal{A}_1 - \frac{2}{3}\mathcal{A}_2 + \frac{4}{3}\mathcal{C}$	0	$\frac{3}{2}$
	③ $70^\circ (XZ)$	$E_Y (\Gamma_2)$	$\mathcal{A}_1 - \frac{2}{3}\mathcal{A}_2 - \frac{4}{3}\mathcal{C}$	$\frac{8}{3}$	$\frac{1}{6}$
	④				
$\langle 110 \rangle$	① $35^\circ (XZ)$	$E_X (\Gamma_1)$	$\mathcal{A}_1 + \mathcal{A}_2 - \mathcal{B} + \mathcal{C}$	0	$\frac{2}{3}$
	②	$E_Y (\Gamma_2)$	$\mathcal{A}_1 + \mathcal{A}_2 + \mathcal{B} - \mathcal{C}$	$\frac{2}{3}$	$\frac{8}{9}$
	③ $90^\circ (YZ)$	$E_X (\Gamma_1)$	$\mathcal{A}_1 - \mathcal{A}_2 - \mathcal{B} - \mathcal{C}$	2	0
	④	$E_Y (\Gamma_2)$	$\mathcal{A}_1 - \mathcal{A}_2 + \mathcal{B} + \mathcal{C}$	0	$\frac{10}{9}$

976 NM TRANSITION

As described in the main text, the qualitative behavior of the 946 nm and 976 nm transitions is identical. However, a small additional transition appears in certain excitation-detection combinations, namely $\pi\pi$ and $\sigma\sigma$ [Fig S3]. As

no other features of the 946 nm system are sensitive to input polarization in these measurements, we attribute this additional peak to an unrelated feature.

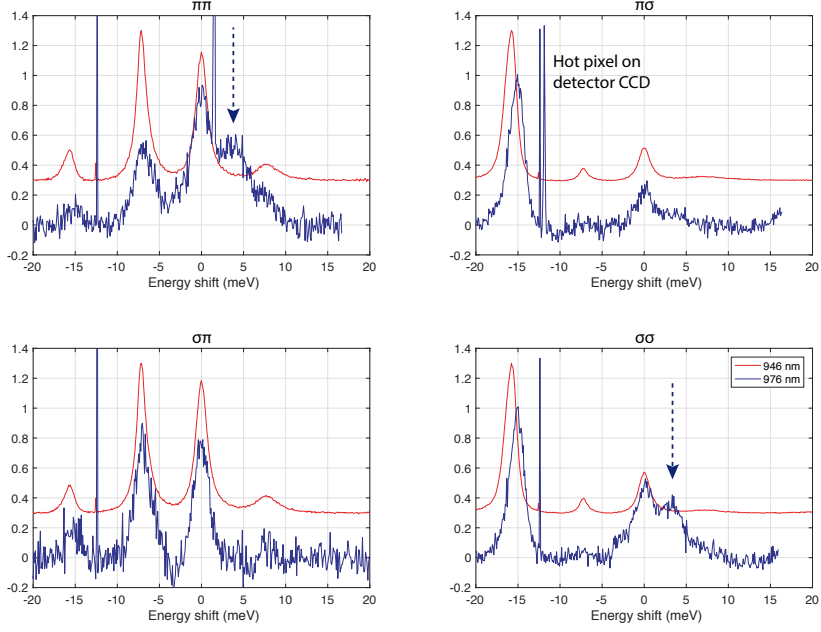


FIG. S3. Comparison of 946 nm spectra (red) with 976 nm spectra under 2.1 GPa of applied $\langle 110 \rangle$ stress. The spectra are labelled with excitation and detection polarization. In each case, spectra are essentially identical except for the feature marked with an arrow in the $\pi\pi$ and $\sigma\sigma$ spectra. No other feature of the SiV^0 system is sensitive to input polarization and therefore we assign it to an unrelated defect emitting close to the 976 nm transition.

SPIN POLARIZATION MECHANISM

The electronic structure of SiV^0 is complex, with three and six electronic states arising from the first two lowest-energy electronic configurations e_g^2 and $e_u e_g$, respectively. Considering only symmetric A_{1g} phonons, the first-order intersystem crossings (ISC) from the triplet manifold to the singlet manifold are given in Fig. S4. In this picture, there are no ISCs from the ${}^3A_{2u}$ to lower-energy singlet states, suggesting spin polarization should decrease at low temperature, contrary to experiment. Additional information on the relative energy and ordering of the singlets is required for further analysis.

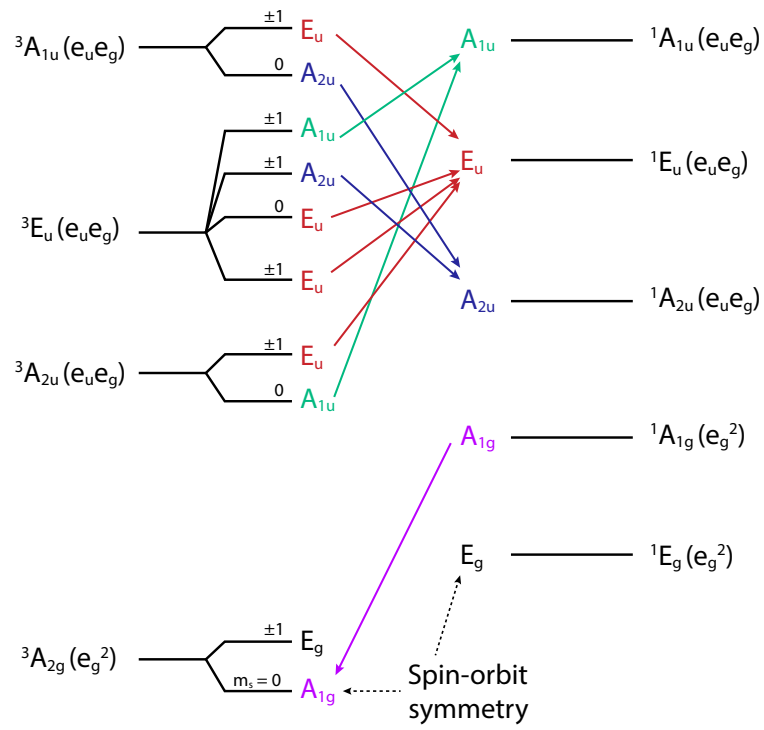


FIG. S4. First-order intersystem crossings involving only A_{1g} phonons. The electronic symmetries are given on the far left and right of the figure, with the spin-orbit symmetry given in the center. The states are ordered according to their Coulomb repulsion energy.

* b.green@warwick.ac.uk; Corresponding Author

- [S1] A. E. Hughes and W. A. Runciman, Proc. Phys. Soc. **90**, 827 (1967).
- [S2] G. Davies, J. Phys. C Solid State Phys. **12**, 2551 (1979).
- [S3] G. Davies and M. E. R. Hamer, Proc. R. Soc. London Ser. A **348**, 285 (1976).
- [S4] K. Mohammed, G. Davies, and A. T. Collins, J. Phys. C Solid State Phys. **15**, 2779 (1982).
- [S5] L. J. Rogers, M. W. Doherty, M. S. J. Barson, S. Onoda, T. Ohshima, and N. B. Manson, New J. Phys. **17**, 013048 (2015).